



HAL
open science

The water vapor self-continuum absorption at room temperature in the 1.25 μm window

. . Koroleva, S. Kassi, Alain Campargue

► To cite this version:

. . Koroleva, S. Kassi, Alain Campargue. The water vapor self-continuum absorption at room temperature in the 1.25 μm window. *Journal of Quantitative Spectroscopy and Radiative Transfer*, 2022, 286, pp.108206. 10.1016/j.jqsrt.2022.108206 . hal-03865615

HAL Id: hal-03865615

<https://hal.science/hal-03865615>

Submitted on 22 Nov 2022

HAL is a multi-disciplinary open access archive for the deposit and dissemination of scientific research documents, whether they are published or not. The documents may come from teaching and research institutions in France or abroad, or from public or private research centers.

L'archive ouverte pluridisciplinaire **HAL**, est destinée au dépôt et à la diffusion de documents scientifiques de niveau recherche, publiés ou non, émanant des établissements d'enseignement et de recherche français ou étrangers, des laboratoires publics ou privés.

1 The water vapor self-continuum absorption at room temperature
2 in the 1.25 μm window

3
4
5 A.O. Koroleva ^{1,2}, S. Kassi ¹ and A. Campargue ¹
6

7
8 ¹ *Univ. Grenoble Alpes, CNRS, LIPhy, Grenoble, France*

9 ² *Institute of Applied Physics of RAS, Nizhniy Novgorod, Russia*
10
11

12
13
14
15
16
17
18
19
20
21
22 *Monday, 11 April 2022*

23 **Key words**

24 Water vapor; continuum absorption; MT_CKD model; CRDS; atmospheric window; water
25 dimer

26
27 Number of Pages: 21

28 Number of Figures: 7

29 Number of Tables: 1
30
31
32
33
34

- 35 • *Corresponding author:* Alain Campargue (Alain.Campargue@univ-grenoble-alpes.fr)

36

Abstract.

37 The water vapor self-continuum is newly measured at room temperature in the high energy edge of the
38 1.25 μm window by using highly stable and sensitive cavity ring down spectroscopy (CRDS). Self-
39 continuum cross-sections, C_S , are derived between 8290 and 8620 cm^{-1} at 29 selected spectral points
40 by using pressure ramps (up to 15 Torr) of pure water vapor. Purely quadratic pressure dependence is
41 obtained for the absorption coefficient at each measurement point. Although the spectral measurement
42 points were chosen to minimize the contribution of resonance line absorption, the latter represents
43 between 30 and 70 % of the measured absorption in the studied region. The measurements are found
44 consistent with a previous study of the low frequency edge of the 1.25 μm windows and (Campargue
45 et al. J Geophys Res Atmos 2016;121:13,180 – 13,203. doi:10.1002/2016JD025531). The frequency
46 dependence of the retrieved C_S values shows an overall good agreement with the MT_CKD values,
47 although an additional broad absorption feature is observed with a center near 8455 cm^{-1} . It is
48 tentatively interpreted as a possible impact of the uncertainties on the resonance line contribution on
49 the derived C_S values or as a possible evidence of a band of the bound dimers, $(\text{H}_2\text{O})_2$.

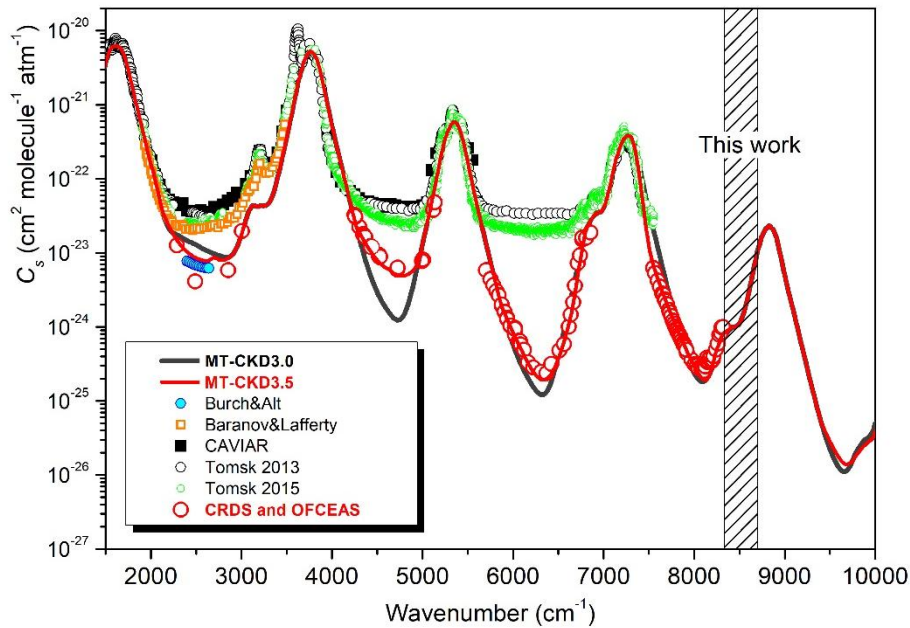
50 **1. Introduction**

51 Water vapor absorption represents more than half of the solar light absorbed by the Earth
52 atmosphere. The water absorption spectrum shows strong rovibrational bands separated by spectral
53 regions of lower opacity, the transparency windows. The water continuum is mostly smooth and
54 structureless and follows a frequency dependence similar to the envelope of the rovibrational
55 spectrum. Although the continuum amplitude sharply decreases in the windows, its relative
56 importance is much higher than in the band regions where the line absorption generally dominates.

57 Note that in the Earth's atmosphere, the water continuum arises from the interaction of water
58 molecules with each other and with other atmospheric molecules (self- and foreign-continuum,
59 respectively). In order to account for the water vapor continuum absorption in atmospheric radiative
60 transfer codes, the semi-empirical MT_CKD model [1], [2], [3] is generally implemented. This model
61 uses an empirical line shape modeling with sub-Lorentzian far wings and a weak interaction term
62 between a water vapor molecule and another molecule for the intermediate wings. The parameters of
63 this empirical line shape have been fitted to a selection of laboratory or field measurements available
64 mostly in the mid infrared (see [2], [4] and references therein).

65 In general, the quantitative determination of weak absorption continua by transmission
66 spectroscopy is generally challenging as continua show up as small decreases of the transmitted
67 spectrum baseline when the absorption cell is filled with the studied gas species. The challenge is
68 made particularly difficult in the case of water vapor because of possible experimental biases due to
69 surface effects (adsorption, condensation) on the optics of the experimental setup. Since the pioneer
70 works of Burch using a grating spectrograph in the 10 μm and 4.0 μm transparency windows [5-7],
71 large experimental efforts have been undertaken to characterize the water self-continuum in the
72 atmospheric windows. Room temperature measurements performed by Fourier transform spectroscopy
73 (FTS) at the Institute of Atmospheric Optics in Tomsk and at RAL (Rutherford Appleton laboratory)
74 within the frame of the CAVIAR (Continuum Absorption at Visible and Infrared wavelengths and its
75 Atmospheric Relevance) [8] were found in good agreement with each other but largely above the
76 MT_CKD values in the 4.0, 2.1 and 1.6 μm windows [9,10]. The overview comparison of the FTS
77 self-continuum cross-sections (C_S) to the corresponding MT_CKD values between 1500 and 9000 cm^{-1}
78 ¹ is presented in **Fig. 1**. The FTS cross-sections have an unexpectedly similar value in the 4.0, 2.1 and
79 1.6 μm windows ($C_S \approx 2 \times 10^{-23} \text{ cm}^2 \text{ molecule}^{-1} \text{ atm}^{-1}$) while the MT_CKD values decrease significantly
80 from the 4.0 window to the 1.6 μm window. As a result, the disagreement reaches two orders of
81 magnitude compared to Tomsk measurements near 1.6 μm [9,10]. In the last years, we have
82 undertaken a characterization of the self-continuum of water vapor using cavity enhanced absorption
83 spectroscopies (CEAS) [11], [12], [13], [14], [15], [16], [17], [18], namely cavity ring down
84 spectroscopy (CRDS) and optical feedback-cavity enhanced absorption spectroscopy (OF-CEAS).
85 These CEAS self-continuum absorption retrievals were all supported by a clear pressure squared
86 dependence of the continuum absorption in order to exclude potential experimental biases. As

87 illustrated in **Fig. 1**, the CEAS measurements sampling the 4.0, 2.1, 1.6 and 1.25 μm windows validate
 88 the overall frequency dependence of the MT_CKD continuum. The 3.0 version of the MT_CKD
 89 continuum, elaborated before the CEAS measurements, nevertheless showed significant deviations, by
 90 up a factor of five in the center of the 2.3 μm window. Starting from the 3.2 version, CEAS cross-
 91 sections were considered as experimental constraints of the MT_CKD continuum (see **Fig. 1**). Note
 92 that it appeared that the CAVIAR and Tomsk room temperature self-continuum values were affected
 93 by reflectivity issues related to the adsorption of water on the optics of the multipass cell used for the
 94 FTS recordings [19], [20].



95
 96 **Fig. 1**

97 Overview comparison of the self-continuum cross-section of water vapor near room temperature between
 98 1500 and 9000 cm^{-1} . Solid lines show different versions of the MT_CKD 3.0 and 3.5 versions at 296 K [3].
 99 Experimental results were obtained by OFCEAS and CRDS (red circles; [11], [12], [13], [14], [15], [16], [17],
 100 [18]); by FTS from [21] (orange open squares), from CAVIAR consortium (black full squares; [8]), from
 101 Tomsk2013 (black open circles; [9]), from Tomsk2015 (green circles; [10]) and with a grating spectrograph by
 102 [6,7] (blue circles). The 8290-8620 cm^{-1} spectral interval presently studied by CRDS is indicated.
 103

104 The physical origin of the water vapor continuum is one of the most long-standing issues in
 105 molecular spectroscopy. Although being mostly based on far-wing line-by-line calculations, the
 106 widely used MT_CKD continuum might account in an operative way for different contributions
 107 including not only deviations of the far wings from calculated profiles but also absorption due to
 108 metastable (quasibound) and stable (truly bound) dimers [22].

109 The experimental evidence of a contribution of bound water dimers (BWD, hereafter) is
 110 difficult as BWD bands are expected to show up as weak unresolved structures, generally overlapping
 111 with the wider envelope of the water monomer (WM) bands and superimposed to the far-wing
 112 continuum whose envelope resembles that of the WM resonance lines.

113 Based on theoretical predictions of the BWD spectrum, different spectral regions have been
 114 considered for detection of BWD spectral signatures in water vapor at thermodynamical equilibrium:

115 (i) Twenty years ago, on the basis of calculations by Low and Kjaergaard [23], the detection of
116 BWD absorption was reported near 750 nm from low resolution spectra recorded in open air
117 atmosphere with an 18.4 km absorption path length over the sea [24]. In spite of a weaker intensity of
118 near-infrared BWD bands, the 750 nm spectral region was targeted as it limits interference with WM
119 absorption. The claimed BWD evidence was obtained by difference of the measured atmospheric
120 absorbance and a simulation of the WM absorption lines relying on the version of the HITRAN
121 database available at that time. Later, a high number of weak WM lines missing in the used HITRAN
122 list were measured by CRDS [25]. The resulting additional absorbance was found to represent an
123 important fraction of the reported BWD atmospheric absorption and questioned the reliability of the
124 BWD detection, which was finally revoked [26].

125 (ii) The mm-submm wave range where the BWD pure rotational spectrum is located, offers an
126 alternative way to minimize the spectral interference between BWD and WM absorption. A series of
127 thirteen quasi-equidistant spectral features recorded in water vapor at room temperature in the 0.1-0.26
128 THz ($3.5\text{-}8.7\text{ cm}^{-1}$) interval [27], [28], [29] was found in good agreement with first principle
129 calculations of transitions computed between all rovibrational states [30]. This observation provided
130 the first definitive detection of BWDs in equilibrium water vapor at room temperature. Moreover,
131 BWDs were confirmed to bring the largest contribution to the room temperature continuum absorption
132 in the considered mm-wave range.

133 (iii) Although the discrimination of BWD absorption in the in-band self-continuum is
134 complicated, strong evidence of BWD signature has been reported in the monomer bending region
135 near 1600 cm^{-1} , in the OH stretching fundamental band near 3700 cm^{-1} and in the region of the stretch-
136 bend combination band near 5300 cm^{-1} [31], [32], [33], [34], [35]. Distinct (broad) spectral peaks were
137 found to coincide with BWD calculated spectrum [23], [36], [37] leaving little doubt on the BWD
138 contribution to the in-band continuum. Very recently, similar comparison between WD predicted
139 spectrum and FTS self-continuum measurements were performed in the region of the bands at 8800
140 and 10600 cm^{-1} [38]. The measurements were performed at high temperature (398 K and 431 K) in
141 order to allow for using high water vapor pressure values (1-4 atm). A dimer-based model including
142 both quasibound and bound WD contributions was developed and found to fit reasonably well to the
143 measured self-continuum. About half of the measured continuum was found to have a WD origin, the
144 quasibound contribution being larger than the BWD contribution for the considered bands [38].

145 The present study is devoted to the first experimental retrieval of the room temperature water
146 vapor self-continuum in the $8290\text{-}8620\text{ cm}^{-1}$ spectral range, thus extending to higher energy our
147 previous CEAS studies. The studied region corresponds to the high energy edge of the $1.25\text{ }\mu\text{m}$
148 window (see **Fig. 1**). The center and low energy range of the window ($7548\text{-}8318\text{ cm}^{-1}$) were
149 previously investigated by CRDS in Ref. [12]. The characterization of the atmospheric absorbers in
150 this particular window is of importance as the $1.27\text{ }\mu\text{m}$ oxygen band (including rovibronic lines
151 superimposed over a broad collision induced absorption (CIA) band - see *e. g.* [39], [40]) is considered

152 for air-mass determination in a number of satellite missions [41]. In addition, near 8500 cm^{-1} , the
153 studied region overlaps the above mentioned FTS investigation at high temperature [38] which will
154 allow for a discussion of the temperature dependence. Finally, a BWD absorption band is predicted
155 with significant intensity in the studied spectral interval and its detection would be the first
156 experimental evidence of the BWD contribution to the continuum in the near infrared transparency
157 windows.

158 In the following Part 2, we will present the experimental procedure and data acquisition. Part 3
159 is devoted to the retrieval of the cross-sections while comparison to the literature, considerations about
160 the temperature dependence and possible detection of a BWD signature are presented in Part 4 before
161 the concluding remarks (Part 5).

162 **2. CRDS measurements**

163 *2.1. CRDS setup*

164 Self-continuum measurements were performed by CRDS at a series of spectral points sampling
165 the $8293 - 8621\text{ cm}^{-1}$ spectral interval. An external cavity diode laser (ECDL) was used as light source.
166 The reader is referred to [42] [43] for the description of the cavity ring down spectrometer and the
167 frequency tuning of the ECDL. Briefly, the ECDL central emission frequency is tuned by changing the
168 laser current together with the grating angle driven by a piezoelectric transducer (PZT). The typical
169 mode-hop free tuning range of the ECDL used here (Toptica fiber-connected DL pro, 1200 nm) is
170 about 0.8 cm^{-1} . The 1.40 m long CRDS cell is fitted by high reflectivity mirrors leading to ring down
171 times of about $350\text{ }\mu\text{s}$ around 8300 cm^{-1} . The setup is fibered and the polarization is maintained up to
172 the optical cavity, providing better reproducibility. The wavenumber of the ECDL is measured by a
173 commercial Fizeau type wavemeter (HighFinesse WSU7-IR, 5 MHz resolution, 20 MHz accuracy
174 over 10 hours) that allows laser frequency to be determined at a typical 100 Hz refresh rate. The laser
175 frequency was stable within 3MHz during the short time of each recording.

176 The output mirror of the cavity is mounted on a piezoelectric transducer to periodically change
177 the cell length allowing covering one free spectral range (FSR) of the cavity and thus achieving
178 resonance between the laser light and one longitudinal mode of the cavity. After a build-up time
179 necessary to fill the cavity with photons at resonance, the injection of laser light is stopped thanks to
180 an acousto-optic modulator and the purely exponential decay time of photons leaking from the cavity
181 (*i.e.* the ring down (RD) time, τ) is measured with a photodiode. The fitted RD time is directly related
182 to the absorption coefficient of the absorbing gas, $\alpha(\nu)$:

$$183 \quad \alpha(\nu) = \frac{1}{c\tau(\nu)} - \frac{1}{c\tau_0(\nu)} \quad (1)$$

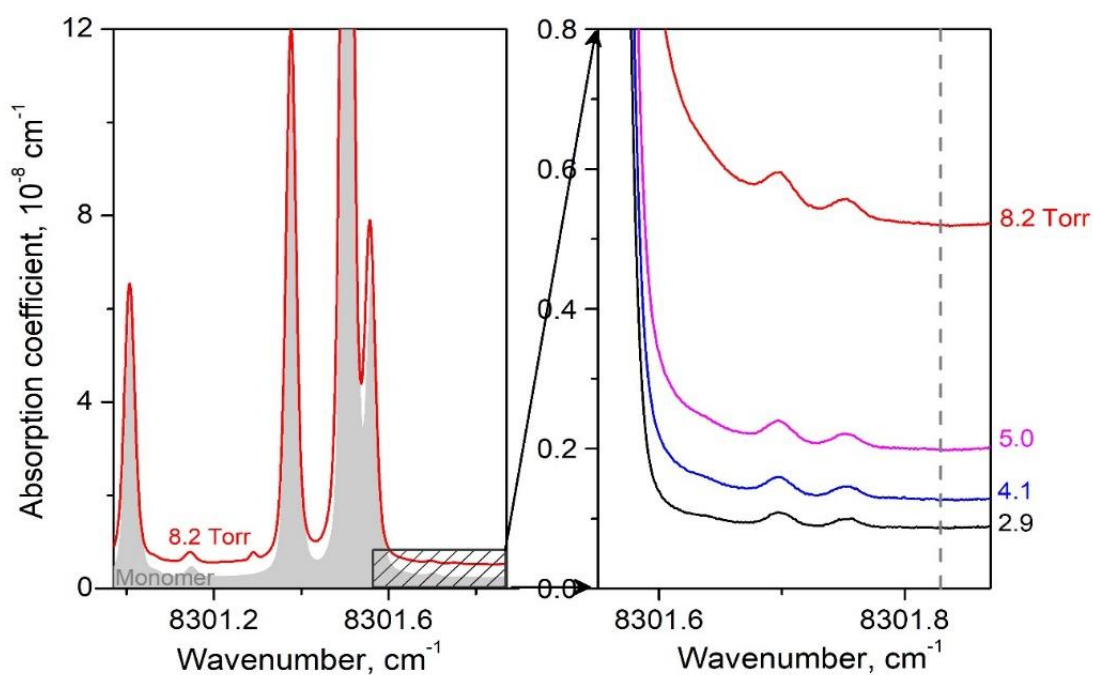
184 where c is the speed of light, ν is the laser frequency. τ_0 and τ are the ring down time with the
185 optical cavity empty, or filled with a non-absorbing gas, respectively.

186 Two pressure gauges (10 and 1000 Torr full scale, from MKS Instruments) were installed on the
187 cavity to continuously measure the total pressure with an accuracy of 0.25% of reading. A temperature

188 sensor (TSic 501 from IST, ± 0.1 K accuracy) was fixed on the external wall of the cavity and
189 enveloped by thermal insulation foam to continuously record the temperature which remained in the
190 294 ± 1 K range during the whole measurement campaign.

191 2.2. Data acquisition

192 As described below, measurements were performed for increasing and decreasing pressure
193 ramps at fixed frequency. We nevertheless present in **Fig. 2** some spectra recorded for different
194 pressure values in order to illustrate how the measurement spectral points were selected. Water
195 continuum is generally much weaker than resonance line contribution, but in well-chosen
196 microwindows of transparency, the continuum may become equivalent to the resonance line
197 absorption or even predominant. This is illustrated in **Fig. 2** in the region of the selected 8301.825 cm^{-1}
198 measurement point. For a pressure of 8.2 Torr, the measured absorption coefficient at 8301.825 cm^{-1}
199 involves equivalent contributions of the self-continuum and of the WM resonance lines (obtained from
200 a spectrum simulation - see below). Note that the far-wing and the self-continuum contributions have
201 both a pressure-squared dependence which makes their relative importance independent on the
202 pressure. On the right panel of **Fig. 2**, the pressure dependence of the spectrum is illustrated for four
203 pressure values ranging from 2.9 to 8.2 Torr. The spectrum baseline (corrected from the empty cavity
204 loss rate) is observed to increase rapidly (in fact, quadratically) with pressure.



205

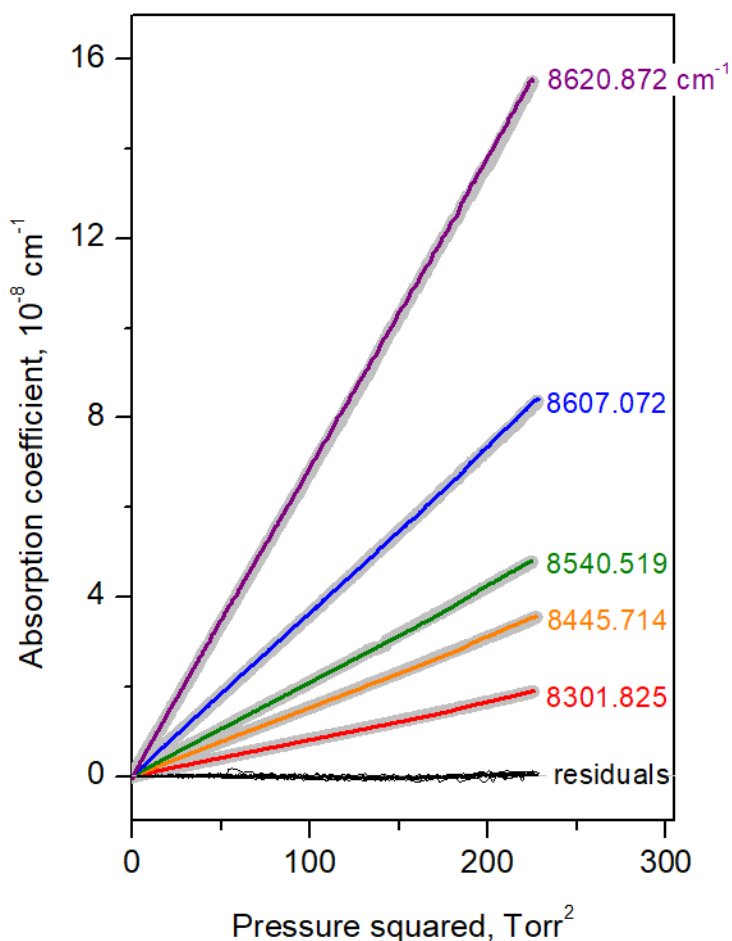
206 **Fig. 2**

207 *Left panel:* Comparison of the CRDS absorption coefficient for water vapor at a pressure of 8.2 Torr with
208 a resonance line simulation modeled using HITRAN2020 [44]. The zero absorption baseline was fixed to the
209 loss rate value obtained with an empty cavity.

210 *Right panel:* Pressure dependence of CRDS spectra of pure water vapor near 8301 cm^{-1} , showing the
211 increase of the baseline level due to water vapor self-continuum (the constant term due to the empty cavity losses
212 was subtracted). The vertical dashed line corresponds to the measurement spectral point at 8301.825 cm^{-1} .

213

214 Twenty-nine spectral points were thus selected far from intense water vapor lines in order to
 215 reduce the impact of the uncertainty of the line parameters which is the main uncertainty source of the
 216 derived cross-sections (see below). The sensitivity of the recordings makes it necessary to consider the
 217 presence of impurities in the water sample. Indeed, NH_3 and CO_2 might be present in the sample with
 218 maximum relative abundances of 5 ppm and 120 ppm, respectively, which makes their strongest
 219 transitions observable in the region. For instance, in the region displayed in **Fig. 2**, a CO_2 and a NH_3
 220 line are visible at 8301.293 cm^{-1} and 8301.756 cm^{-1} , respectively. At the chosen spectral points, the
 221 CO_2 and NH_3 line contributions are all less than 0.1% of the total absorption and can be neglected.
 222



223 **Fig. 3.**
 224 Self-continuum absorption *versus* the squared water vapor pressure during pressure ramps up to 15 Torr
 225 for different spectral points of the $1.25 \mu\text{m}$ window. For each spectral point, measurements were performed
 226 during increasing and decreasing pressure ramps (grey and colored lines, respectively). The self-continuum
 227 cross-section values were derived from the linear fits. The residuals (black line) correspond to the superposition
 228 of the differences between measurements and the five linear fits.
 229
 230

231 At the beginning of each day of measurements, the water sample was purified by cooling with
 232 liquid nitrogen and evacuating the residual vapor phase. For each selected spectral point, the
 233 absorption coefficient was recorded during an increasing pressure ramp from 0 to 15 Torr (*i.e.* about
 234 71% of the saturation pressure at 296 K) followed by a decreasing pressure ramp. The pressure was
 235 varied at a speed of about 0.1 Torr/second in order to limit the influence of adsorption and desorption

236 effects which become noticeable at lower speed. The typical duration of the pressure cycle was 6-7
237 minutes.

238 Some measurements were repeated several times to check the repeatability. The linear
239 dependence of the absorption coefficient *versus* pressure squared is illustrated in **Fig. 3** for five
240 spectral points (Note that the residuals displayed on the figure correspond to the superposition of the
241 five linear fits of the measurements). A very good coincidence is obtained for the measurements
242 performed during increasing and decreasing pressure ramps (grey and colored lines, respectively).

243 2.3. Self-continuum cross-sections retrieval

244 The absorption coefficient, α , as defined in Eq. (1) can be expressed as:

$$245 \alpha(\nu, T) = \alpha_{WML} + \alpha_{WCS} = \alpha_{WML} + \frac{1}{kT} C_S(\nu, T) P_{H_2O}^2 \quad (2)$$

246 where k is the Boltzmann constant, α_{WML} and α_{WCS} are the contributions due to resonant lines
247 (WML) and the water vapor self-continuum (WCS), respectively. C_S is the self-continuum cross-
248 sections expressed in $\text{cm}^2 \text{molecule}^{-1} \text{atm}^{-1}$. Note that the Rayleigh scattering which is proportional to
249 pressure and omitted in Eq. (2) was estimated and found negligible (at 15 Torr, Rayleigh scattering
250 losses are less than two orders of magnitude smaller than the total absorption coefficient, α).

251 A simulation of the water vapor rovibrational spectrum, α_{WML} , was performed at different
252 pressures on the basis of the HITRAN2020 line list [44], using a Voigt profile and the standard wings
253 cut-off at 25 cm^{-1} frequency detuning from the line center (the underlying pedestal is considered as
254 part of the continuum for easier comparison with MT_CKD and other studies). For each spectral point,
255 the proportionality factor between α_{WML} and $P_{H_2O}^2$ was determined and subtracted from the fitted slope
256 of the absorption coefficient *versus* $P_{H_2O}^2$ (**Fig. 3**). The resulting value, $\frac{1}{kT} C_S(\nu, T)$, leads to the cross-
257 sections listed in **Table 1** and presented in **Fig. 4**. For some spectral points, several pressure ramps (up
258 to 4 – see **Table 1**) were performed and the listed C_S values and corresponding statistical error bars
259 result from the global fit of the different recordings. The statistical error resulting of the linear fit of α
260 *versus* $P_{H_2O}^2$ is included in **Table 1**.

261

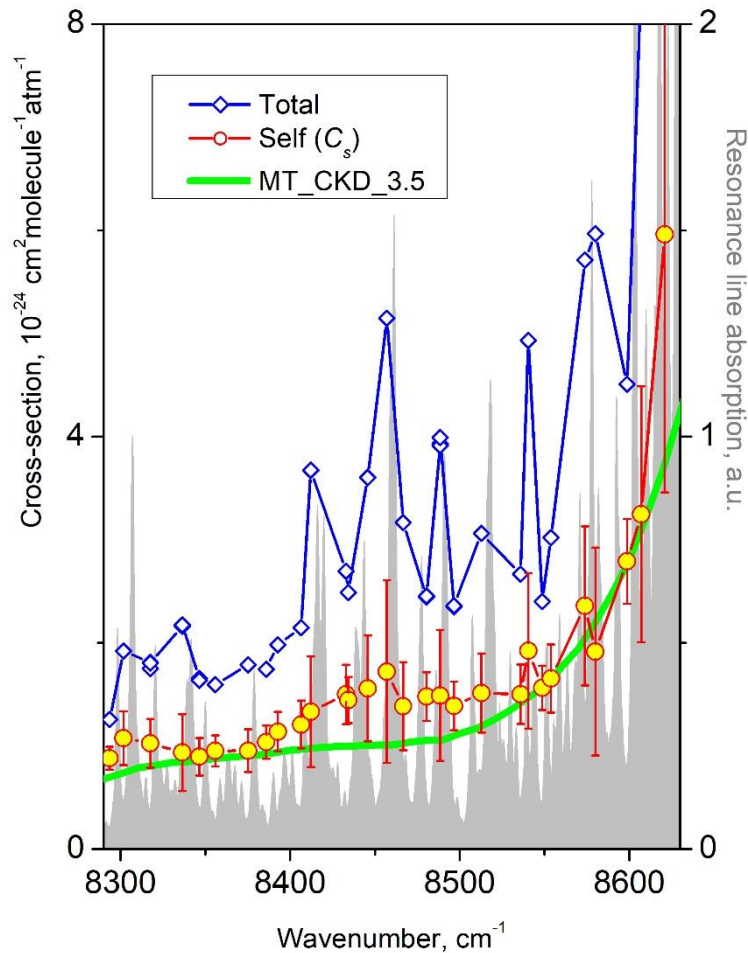
262 **Table 1.**
 263 Self-continuum cross sections of water vapor at room temperature (294 K) derived between 8293 and
 264 8621 cm^{-1} .
 265

Frequency cm^{-1}	C_s^a $10^{-24} \text{ cm}^2 \text{ molecule}^{-1} \text{ atm}^{-1}$	R_{WML}^b %	$C_s \text{ Unc}^c$ %	Nb of ramps
8293.592	0.883(1)	29.7	12.6	1
8301.825	1.076(1)	44.0	24.3	2
8317.615	1.026(27)	42.7	22.8	3
8336.464	0.937(7)	56.8	39.7	2
8346.523	0.896(9)	45.6	20.2	2
8355.863	0.953(2)	40.3	15.7	1
8375.201	0.955(3)	46.6	21.6	1
8385.874	1.038(3)	40.5	15.5	1
8392.751	1.140(3)	42.5	16.8	1
8406.511	1.208(3)	42.5	19.2	1
8412.218	1.333(3)	63.7	40.2	2
8432.946	1.501(3)	44.3	19.2	1
8434.240	1.446(3)	41.9	15.4	1
8445.714	1.559(3)	56.8	33.0	2
8456.934	1.722(3)	66.5	51.5	1
8466.674	1.386(3)	56.3	30.8	1
8480.505	1.480(7)	39.6	16.0	2
8488.515	1.49(3)	62.2	42.6	4
8496.624	1.388(6)	41.1	17.0	2
8512.892	1.513(2)	50.6	25.3	2
8535.871	1.503(4)	43.6	19.2	1
8540.519	1.923(3)	61.0	39.2	1
8548.646	1.565(3)	34.9	13.7	2
8553.827	1.656(3)	45.2	19.9	1
8573.765	2.360(4)	58.7	32.7	1
8579.992	1.916(3)	67.9	52.7	2
8598.690	2.791(4)	38.1	14.7	1
8607.072	3.247(4)	61.9	38.2	1
8620.872	5.960(68)	62.8	41.9	3

266
 267
 268 Notes
 269 ^a The statistical uncertainties are given within parentheses after each C_s value, in the unit of the last quoted digit.
 270 They include the fit uncertainty and statistical uncertainty (for the frequencies where measurements were
 271 repeated – see last column). The uncertainties related to the resonant line subtraction are much larger and
 272 included in the column total uncertainties given in the “ $C_s \text{ Unc}$.” column.
 273 ^b Relative contribution of the far-wing contribution to the total measured absorption coefficient: $\alpha_{WML} =$
 274 $\alpha_{WML} / (\alpha_{WML} + \alpha_{WCS})$.
 275 ^c Total uncertainty on the retrieved C_s values (in %) mainly due to uncertainty on the (subtracted) far-wing, α_{WML}
 276 (see Text).

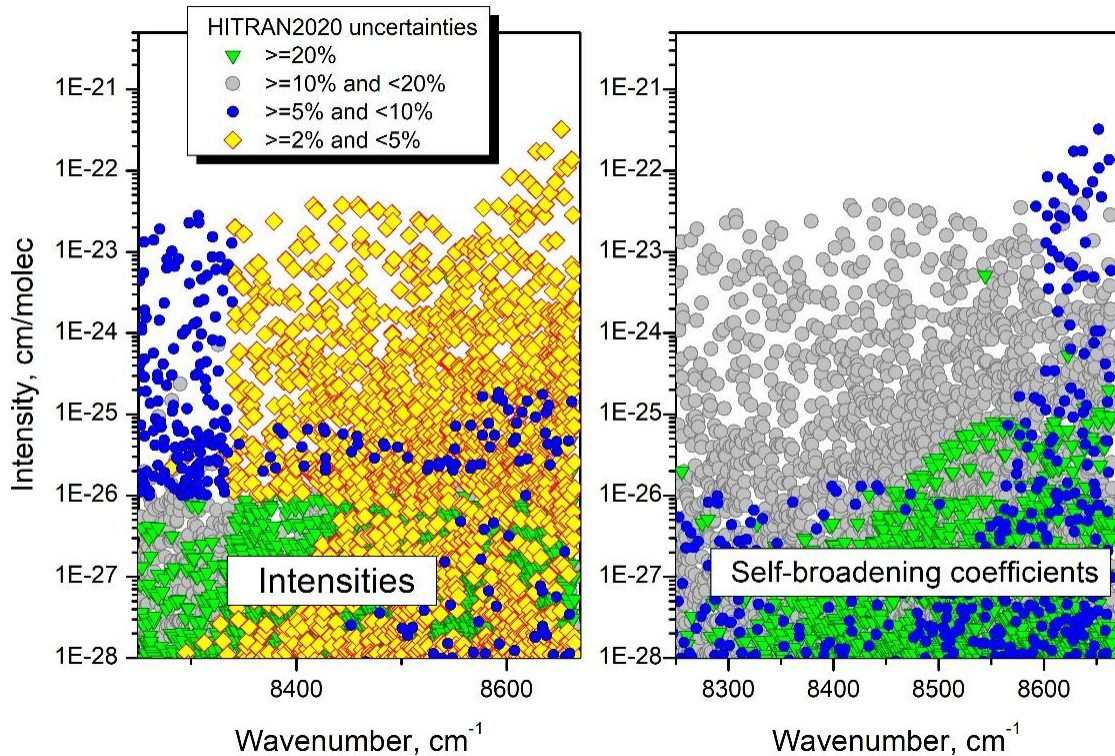
277 The self-continuum cross-sections are compared to the total measured cross-sections in **Fig. 4**.
 278 The difference corresponds to the WM resonant lines whose relative contribution to the total
 279 absorption, $R_{WML} = \alpha_{WML} / (\alpha_{WML} + \alpha_{WCS})$, is given in **Table 1** for each spectral point. Although spectral
 280 points were chosen to minimize α_{WML} as much as possible, the contribution of rovibrational lines is
 281 always important in the considered region and fluctuates between 30% and 70%, according to the
 282 spectral point. It is worth noting that, as expected, the large dispersion of the measured total cross-
 283 sections is significantly reduced after subtraction of the far-wing contributions.

284 While the sum of the self-continuum and resonant line contributions is known experimentally
 285 with an accuracy better than 1% (see **Fig. 3**) accuracy, the uncertainties on the C_S values are much
 286 larger if the uncertainty related to the subtracted resonant line contribution is taken into account. This
 287 is a common situation when WM resonant lines represent a significant fraction of the measured
 288 continuum and the corresponding WM line parameters are not accurately known (see *e.g.* [45]).



289
 290 **Fig. 4**
 291 Total measured cross-section of water vapor at room temperature (blue) at the measurement points
 292 selected in the 1.25 μm window. The residuals obtained after subtraction of the contribution of the resonant lines
 293 are the self-continuum absorption cross-sections (red open circles) which are plotted with their associated total
 294 error bars (dominated by the uncertainties on the resonant lines contribution). The plot includes the
 295 MT_CKD_3.5 values (green line) [3]. For comparison, a low resolution simulation of the resonance absorption
 296 cross-section is presented as grey background.

297 The uncertainty related to the line parameters can be evaluated by propagation of the
 298 uncertainties provided by HITRAN2020 for the different line parameters. In practice, only the
 299 uncertainties on the line intensities (S) and on the self-broadening coefficients (γ_{self}) have a significant
 300 impact. We have plotted in **Fig. 5** the HITRAN2020 line list with a colour depending on their
 301 HITRAN error code. It appears that the error code on γ_{self} corresponds to an uncertainty between 10
 302 and 20 % for most of the lines. The uncertainties on the intensities of the lines of importance are in
 303 the 5-10 % and 2-5 % ranges below and above 8340 cm^{-1} , respectively. As illustrated by their
 304 frequency dependence, HITRAN uncertainties should be considered as rough estimates. Considering
 305 that α_{WML} at a frequency detuned from the line center is simply proportional to γ_{self} and S , their
 306 relative uncertainties propagate unchanged on α_{WML} . Based on the above HITRAN uncertainties, we
 307 roughly take an overall (probably conservative) value of 20 % for the α_{WML} uncertainty which leads to
 308 a relative error on C_S of $20\% \times R_{WML}/(1 - R_{WML})$. As the R_{WML} values range between 35 and 68 %,
 309 we obtain uncertainty values on C_S ranging between about 8 and 42 %, typically one order of
 310 magnitude larger than the uncertainty on the measured total absorption coefficient ($\alpha_{WML} + \alpha_{WCS}$). A
 311 more rigorous treatment by propagation of the HITRAN uncertainties and taking into account of the
 312 statistical uncertainties leads to total uncertainty values ranging between 12 and 53% (see **Table 1**).



313

314 **Fig. 5**

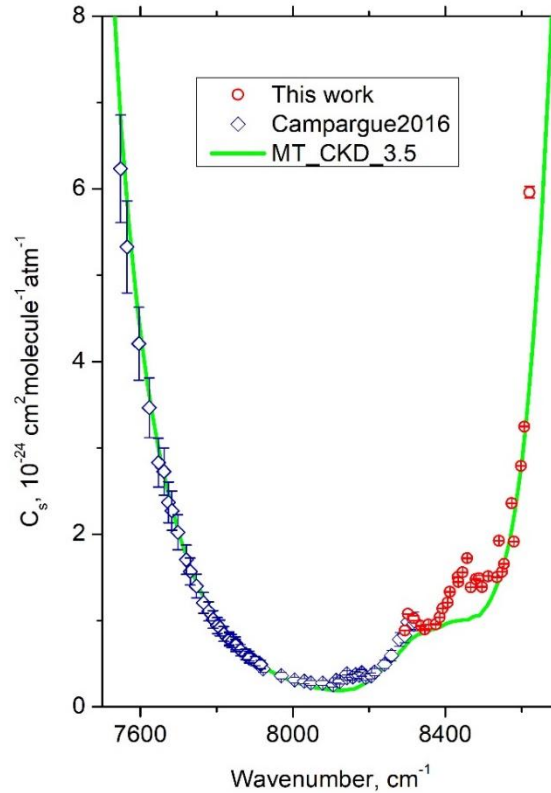
315 Overview of the HITRAN2020 [44] line list of water vapor in the studied region with different symbols
 316 according to the error bar on the line intensities and self broadening coefficients (left and right panels,
 317 respectively).

318

319 **3. Discussion**

320 *3.1. Comparison to literature values.*

321 The retrieved C_S values listed in **Table 1** are plotted in **Fig. 6** together with the previous CRDS
322 measurements below 8310 cm^{-1} [12] and compared to the MT_CKD_3.5 [3] values. It is worth
323 mentioning that as in [12], the plotted experimental error bars do not include the uncertainty due to the
324 resonant lines estimated above.



325

326 **Fig. 6**

327 Self-continuum cross-sections of water vapor at room temperature in the $1.25\text{ }\mu\text{m}$ window. The
328 experimental values measured in [12] and in this work (blue and red circles, respectively) are compared to the
329 MT_CKD_3.5 values. Note that the plotted error bars do not include the (large) contribution due to the resonant
330 lines (see **Table 1** and **Fig. 4** for the total error bars).

331

332 The first three measurement points near 8300 cm^{-1} are in common with those of Ref. [12]. The
333 present values are larger by 6.3, 8.4 and 6.5 % compared to [12]. These deviations are compatible with
334 the combined error bars on the two C_S determinations, on the order of 5.7, 9.5 and 10.0 %, respectively.
335 Nevertheless, the agreement is in fact better than reflected by the 7% average deviation
336 between the two determinations. Half of the disagreement is related to the different versions of the
337 HITRAN database used to calculate the resonance line contribution, α_{WML} . As reflected by the
338 $\alpha_{WML}/(\alpha_{WML} + \alpha_{WC})$ relative contribution values given in [12] and in **Table 1** for the three measurements
339 in common, the resonance line contributions based on HITRAN2012 are larger by about 3% compared
340 to the present values based on the HITRAN2020 version. This example illustrates the correlation
341 between the retrieved continuum cross-section values and the line list used to calculate α_{WML} in the

342 spectral regions where WM resonance line contribution is important. In principle, published C_S values
343 should be used with the same line list as that adopted for the C_S retrieval from the measurements.

344 The comparison with the MT_CKD_3.5 model shows an overall very good agreement. Below
345 8300 cm^{-1} , the MT_CKD model has been refined according to [12] (see **Fig. 1**) but above this value,
346 the present MT_CKD_3.5 version is identical to previous versions and thus independent on our
347 previous CEAS measurements (no other room temperature measurements are available in the $1.25\text{ }\mu\text{m}$
348 window). The observed agreement is thus a convincing validation of the extrapolation capabilities of
349 the MT_CKD towards high energy for practical applications.

350 3. 2. *The structure observed around 8450 cm^{-1}*

351 The comparison to MT_CKD reveals nevertheless an additional broad structure around 8455
352 cm^{-1} (another weaker one seems to be present near 8300 cm^{-1} , although in coincidence with a small
353 local maximum of the MT_CKD values). According to our evaluation of the total uncertainty of the
354 measurement points near 8450 cm^{-1} , the observed weak structure seems to be significant. Two possible
355 explanations are proposed for observed structure. The first one is related to the subtraction of the
356 resonance line contribution while the second is the possible evidence of a spectral signature of the
357 water dimer.

358 According to **Fig. 4**, the spectral measurement points around 8450 cm^{-1} correspond to a
359 relatively large contribution of the resonance line absorption, α_{WML} , which makes the retrieved self-
360 continuum very sensitive to the subtraction of the WM resonance lines (as reflected by the important
361 error bars of the C_S values in the region- see **Fig. 6**). As an additional test of this sensitivity, we
362 performed simulations of α_{WML} changing the usual $\pm 25\text{ cm}^{-1}$ cut off of the plinth to $\pm 5\text{ cm}^{-1}$. This
363 change leads to a decrease of α_{WML} and thus a general increase of the retrieved C_S values. In the
364 region of interest near 8455 cm^{-1} , the resulting increase shows some faint additional structure but the
365 scattering of the obtained C_S values makes it difficult to correlate with the observed structure. Let us
366 underline that the structure was obtained following the usual $\pm 25\text{ cm}^{-1}$ convention of the MT_CKD
367 model and thus constitutes a deviation from the model, even if it is related to the resonance line
368 subtraction.

369 As mentioned in the introduction, water dimers contribute to the self-continuum absorption and
370 have been evidenced as broad spectral signatures in the near infrared in-band regions and as partially
371 resolved rotational spectrum in the mm-submm wave range [27], [28]. Our tentative interpretation of
372 the structure near 8455 cm^{-1} as a BWD band will follow the same approach based on a comparison
373 with theory, as applied in [34], [46], [35], [38].

374 By considering the dimer as two individually vibrating monomer units, Salmi et al. calculated
375 variationally the O-H stretching vibrational overtone spectrum with a computed dipole moment
376 surface and an internal coordinate Hamiltonian [37]. According to these calculations, a BWD band is
377 predicted near 8530 cm^{-1} . The vibrational assignment of the BWD upper state of the band, labeled $|0\rangle_f$

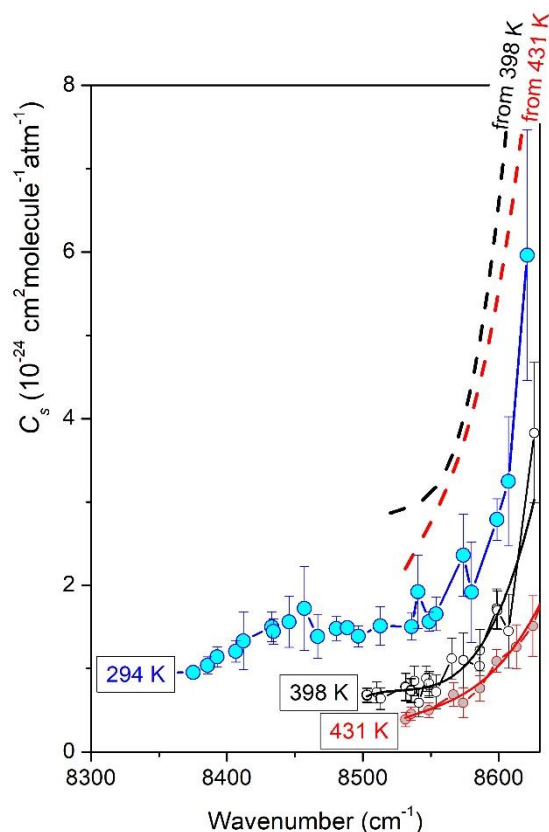
378 $|2>_b|1>$ in [37], corresponds to a vibration of the donor H_2O unit of the $(\text{H}_2\text{O})_2$ dimer, with double
 379 excitation of the bond OH stretch and a single excitation of the H_fOH_b . Although shifted by about 75
 380 cm^{-1} from the centre of the observed absorption feature, this band is the only band predicted in the
 381 region. It is located on the low energy range of a strong band system around 8800 cm^{-1} dominated by a
 382 stretch-bend band of the H_2O acceptor unit ($|20>_a|1>$ in the notation of [37]), which is predicted about
 383 33 times stronger than the donor acceptor band near 8530 cm^{-1} . Intensity considerations provide an
 384 additional insight. The BWD cross-section integrated over a given band is simply the product of the
 385 BWD band intensity, S_{band} in $\text{cm}/\text{molecule}$ units, by the bond dimer equilibrium constant, K_{eq}^b (in atm^{-1})
 386 (see *e.g.* Eq. (3)) in [38]:

$$387 \quad \int C_S dv = K_{eq}^b S_{band} \quad (2)$$

388 According to [38], the intensity of the BWD band predicted at 8530 cm^{-1} [37], is 2.35×10^{-21}
 389 $\text{cm}/\text{molecule}$ while the value of the equilibrium constant at room temperature is about 0.025 atm^{-1} . It
 390 leads to a calculated value of $5.87 \times 10^{-23} \text{ cm} \times \text{molecule}^{-1} \text{ atm}^{-1}$ for the integrated cross-section of the
 391 band at 8530 cm^{-1} . This value can be compared to the experimental value which is obtained from a
 392 Gaussian fit of the experimental values after subtraction of the MT_CKD baseline. An experimental
 393 value of $(4.89 \pm 1.3) \times 10^{-23} \text{ cm} \times \text{molecule}^{-1} \text{ atm}^{-1}$ is obtained in good agreement with the predicted value,
 394 although the coincidence might be coincidental (Note that the center and width (HWHM) values
 395 provided by the fit are $8455.2 \pm 3.4 \text{ cm}^{-1}$ and $38.4 \pm 5.8 \text{ cm}^{-1}$, respectively).

396 4.3. Temperature dependence

397 As mentioned in the introduction, the spectral coverage of the high temperature FTS study of
 398 [38] overlaps the present measurements in the $8500\text{-}8620 \text{ cm}^{-1}$ interval. The water vapor self-
 399 continuum is known to decrease sharply with temperature, contrary to the foreign-continuum which is
 400 much less sensitive to temperature. In the 4.0 and $2.1 \mu\text{m}$ transparency windows, the CEAS
 401 measurements near room temperature combined with high temperature CAVIAR values have provided
 402 clear evidence of a $C_S(T)$ temperature dependence following a simple $\exp\left(\frac{D_0}{kT}\right)$ function where D_0 is
 403 the dissociation energy of the water dimer, $D_0 = 1105(10) \text{ cm}^{-1}$ [47] (see Fig.7 of Ref. [14], Fig.6 of
 404 [13], Fig. 6 of [17]). The situation in the $1.6 \mu\text{m}$ window is less clear, extrapolations of the high-
 405 temperature CAVIAR cross-sections leading to values larger than measured by CEAS near room
 406 temperature (see Fig. 8 in [11]).



407
408
409
410
411
412
413
414

Fig. 7

Self-continuum cross-sections of water vapor between 8475 and 8630 cm^{-1} measured at room temperature (blue circles, this work) and at 398 K and 431 K [38] (black and red circles, respectively). A third order polynomial fit of the 398 K and 431 K datasets (black and red solid lines, respectively) is extrapolated to room temperature following a $\exp\left(\frac{D_0}{kT}\right)$ temperature dependence datasets (black and red dashed lines, respectively). The plotted error bars include the contribution due to the resonant lines for the three datasets

415 The present room temperature cross-sections are plotted in **Fig. 7** with the 398 K and 431 K
416 values of [38] between 8475 and 8630 cm^{-1} . A third order polynomial fit of the frequency dependence
417 of the 398 K and 431 K datasets was performed and the fitted curve was extrapolated to room
418 temperature assuming a $\exp\left(\frac{D_0}{kT}\right)$ temperature dependence. The 398 K and 431 K extrapolations are
419 close to each other but largely above our room temperature C_s values (roughly by a factor of 2).
420 Although this observation should be taken with much caution, considering the error bars of the three
421 sets of measurements considered, the situation shows some similarity to that encountered in the 1.6
422 μm window.

423
424

5. Conclusion

425 The very weak cross-sections of the water vapor self-continuum have been measured by CRDS,
426 using pressure ramps at 29 selected spectral points of the high energy edge of the 1.25 μm window.
427 The pure quadratic pressure dependence of the measured absorption coefficients was found to be
428 accurately fulfilled (see **Fig. 3**) and coinciding results were obtained during increasing and decreasing
429 pressure ramps. As the measured continuum includes an important contribution (30 - 70 %) of the far-

430 wings of the resonance lines, α_{WML} , uncertainties on the resonance line parameters directly impact the
431 accuracy of the derived cross-sections which show a dispersion largely above the experimental
432 accuracy of the CRDS measurements (on the order of 1%).

433 The measurements which are the first measurements at room temperature in the studied range,
434 are found consistent with a previous CRDS study in the low frequency edge of the 1.25 μm window
435 [12]. The MT_CKD model is mostly validated in the region but an additional broad absorption feature
436 is observed with a center near 8455 cm^{-1} . Although the observed absorption peak could be due to an
437 inaccurate subtraction of the resonant line lines, an alternative explanation as a band of the bound
438 dimers, $(\text{H}_2\text{O})_2$ has been discussed. The observed peak is centered about 75 cm^{-1} above the value
439 predicted by theoretical calculations [37]), while the band intensity is found in good coincidence with
440 theory. If this assignment was confirmed, it would be the first experimental evidence of a $(\text{H}_2\text{O})_2$
441 contribution to the water continuum in near infrared transparency. Such an interpretation is consistent
442 with the evidence of strong $(\text{H}_2\text{O})_2$ bands accounting for an important fraction of the continuum in the
443 in-band regions [34], [46], [35], [38] and in the rotational range [27], [28].

444

445 *Acknowledgements*

446 This work is supported by CNRS (France) in the frame of the International Research Project "SAMIA"
447 This work is supported by the French National Research Agency in the framework of the "Investissements
448 d'avenir" program (ANR-15-IDEX-02).

References

- 449
450 [1]
451 Clough SA, Kneizys FX, Davies RW. Line shape and the water vapor continuum. *Atm Res* 1989;23:229-
452 241. doi:10.1016/0169-8095(89)90020-3
453
454 [2]
455 Mlawer EJ, Payne VH, Moncet J, Delamere JS, Alvarado MJ, Tobin DC. Development and recent
456 evaluation of the MT_CKD model of continuum absorption. *Phil Trans R Soc A* 2012;370:2520–2556.
457 doi:10.1098/rsta.2011.0295
458
459 [3]
460 http://rtweb.aer.com/continuum_description.html
461
462 [4]
463 Mlawer EJ, Turner DD, Paine SN, Palchetti L, Bianchini G, Payne VH, Cady-Pereira KE, Pernak RL,
464 Alvarado MJ, Gombos D, Delamere JS, Mlynyczak MG, Mast JC. Analysis of water vapor absorption in
465 the far-infrared and submillimeter regions using surface radiometric measurements from extremely
466 dry locations. *J Geophys Res-Atmos* 2019;124(14):8134–60 doi.org/10.1029/2018JD029508
467
468 [5]
469 Burch DE. Continuum absorption by H₂O. Air Force Geophys Laboratory, Hanscom AFB, MA
470 1982;Report AFGL-TR-81-0300.
471
472 [6]
473 Burch DE, Alt RL. Continuum absorption by H₂O in the 700 – 1200 cm⁻¹ and 2400 – 2800 cm⁻¹
474 windows. Air Force Geophys Laboratory, Hanscom AFB, MA 1984;Report AFGL-TR-84-0128.
475
476 [7]
477 Burch DE. Absorption by H₂O in narrow windows between 3000 and 4200 cm⁻¹. Air Force Geophys
478 Laboratory, Hanscom AFB, MA 1985;Report AFGL-TR-85-0036.
479
480 [8]
481 Ptashnik IV, McPheat RA, Shine KP, Smith KM, Williams RG. Water vapor self-continuum absorption
482 in near-infrared windows derived from laboratory measurements. *J Geophys Res* 2011;116: D16305.
483 doi:10.1029/2011JD015603
484
485 [9]
486 Ptashnik IV, Petrova TM, Ponomarev YN, Shine KP, Solodov AA, Solodov AM. Near-infrared water
487 vapor self-continuum at close to room temperature. *J Quant Spectrosc Radiat Transf* 2013;120:23–
488 35. doi:10.1016/j.jqsrt.2013.02.016
489
490 [10]
491 Ptashnik IV, Petrova TM, Ponomarev YN, Solodov AA, Solodov AM. Water vapor continuum
492 absorption in near-IR atmospheric windows. *Atmos Oceanic Opt* 2015;28:115–120.
493 doi:10.1134/S102485601502009
494
495 [11]
496 Mondelain D, Manigand S, Manigand S, Kassi S, Campargue A. Temperature de- pendance of the
497 water vapor self-continuum by cavity ring-down spectroscopy in the 1.6 μm transparency window. *J*
498 *Geophys Res Atmos* 2014;119(9):2169–8996. doi: 10.1002/2013JD021319.
499
500 [12]

501 Campargue A, Kassi S, Mondelain D, Vasilchenko S, Romanini D. Accurate laboratory determination
502 of the near infrared water vapor self-continuum: A test of the MT_CKD model. *J Geophys Res Atmos*
503 2016;121:13,180 – 13,203. doi:10.1002/2016JD025531
504
505 [13]
506 Richard L, Vasilchenko S, Mondelain D, Ventrillard I, Romanini D, Campargue A. Water vapor self-
507 continuum absorption measurements in the 4.0 and 2.1 μm transparency windows. *J Quant*
508 *Spectrosc Radiat Transf* 2017;201:171–179. doi: 10.1016/j.jqsrt.2017.06.037
509
510 [14]
511 Lechevallier L, Vasilchenko S, Grilli R, Mondelain D, Romanini D, Campargue A. The water vapor self-
512 continuum absorption in the infrared atmospheric windows: new laser measurements near 3.3 and
513 2.0 μm . *Atmos Meas Tech* 2018;11:2159–2171. doi:10.5194/amt-11-2159-2018
514
515 [15]
516 Mondelain D, Vasilchenko S, Čermák P, Kassi S, Campargue A. The self- and foreign-absorption
517 continua of water vapor by cavity ring-down spectroscopy near 2.35 μm . *Phys Chem Chem Phys*
518 2015;17:17,762–17,770. doi: 10.1039/c5cp01238d
519
520 [16]
521 Vasilchenko S, Campargue A, Kassi S, Mondelain D. The water vapor self- and foreign-continua in the
522 1.6 μm and 2.3 μm windows by CRDS at room temperature. *J Quant Spectrosc Radiat Transf*
523 2019;227:230–238. doi: 10.1016/j.jqsrt.2019.02.01
524
525 [17]
526 Ventrillard I, Romanini D, Mondelain D, Campargue A. Accurate measurements and temperature
527 dependence of the water vapor self-continuum absorption in the 2.1 μm atmospheric window. *J*
528 *Chem Phys* 2015;143:134304. doi: 10.1063/1.4931811
529
530 [18]
531 Fleurbaey H, Grilli R, Mondelain D, Campargue A. Measurements of the water vapor continuum
532 absorption by OFCEAS at 3.50 μm and 2.32 μm . *J Quant Spectrosc Radiat Transf* 2022;278:108004.
533 doi.org/10.1016/j.jqsrt.2021.108004
534
535 [19]
536 Ptashnik IV, Solodov AA, Solodov AM.: FTS measurements of the water vapor continuum absorption
537 in 2.1 μm atmospheric window. The XIX Symposium on High Resolution Molecular Spectroscopy 1–5
538 July 2019, Nizhny Novgorod. https://symp.iao.ru/files/symp/hrms/19/presentation_11485.pdf,
539
540 [20].
541 Elsey J, Coleman MD, Gardiner TD, Menang KP, Shine KP. Atmospheric observations of the water
542 vapor continuum in the near-infrared windows between 2500 and 6600 cm^{-1} . *Atmos Meas Tech*
543 2020;13:2335–2361. <https://doi.org/10.5194/amt-13-2335-2020>
544
545 [21]
546 Baranov YI, Lafferty WJ. The water-vapor continuum and selective absorption in the 3-5 μm spectral
547 region at temperatures from 311 to 363 K. *J Quant Spectrosc Radiat Transf* 2011;112:1304-1313.
548 doi:10.1016/j.jqsrt.2011.01.024, 2011.
549
550 [22]

551 Camy-Peyret C, Vigasin AA. Weakly Interacting Molecular Pairs: Unconventional Absorbers of
552 Radiation in the Atmosphere. Dordrecht: Kluwer Academic; 2003, p. 287. (NATO ARW Proceedings
553 Series)
554
555 [23]
556 Low GR, Kjaergaard HG. Calculation of OH-stretching band intensities of the water dimer and trimer.
557 J Chem Phys 1999;110:9104. <https://doi.org/10.1063/1.478832>
558
559 [24]
560 Pfeilsticker K, Lotter A, Peters C, Bösch H. Atmospheric detection of water dimers via near-infrared
561 absorption. Science 2003;300:2078–80. DOI: 10.1126/science.1082282
562
563 [25]
564 Kassi S, Macko P, Naumenko O, Campargue A. The absorption spectrum of water near 750 nm by
565 CW-CRDS: contribution to the search of water dimer absorption. Phys Chem Chem Phys
566 2005;7:2460–7. <https://doi.org/10.1039/B502172C>
567
568 [26]
569 Lotter A. PhD thesis. Heidelberg University; 2006. 156 P.
570
571 [27]
572 Tretyakov MYu, Serov EA, Koshelev MA, Parshin VV, Krupnov AF. Water Dimer Rotationally Resolved
573 Millimeter-Wave Spectrum Observation at Room Temperature. Phys Rev Lett 2013;110:093001.
574 <http://doi.org/10.1103/PhysRevLett.110.093001>
575
576 [28]
577 Serov EA, Koshelev MA, Odintsova TA, Parshin VV, Tretyakov Myu. Rotationally resolved water dimer
578 spectra in atmospheric air and pure water vapor in the 188–258 GHz range. Phys Chem Chem Phys
579 2014;16:26221. <http://doi.org/10.1039/c4cp03252g>.
580
581 [29]
582 Koshelev MA, Leonov II, Serov EA, Chernova AI, Balashov AA, Bubnov GM, An- driyanov AF, Shkaev
583 AP, Parshin VV, Krupnov AF, Tretyakov MY. New fron- tiers in modern resonator spectroscopy. IEEE
584 Trans Terahertz Sci Technol 2018;8:773–83. doi: 10.1109/TTHZ.2018.2875450
585
586 [30]
587 Scribano Y, Leforestier C. Contribution of water dimer absorption to the millimeter and far infrared
588 atmospheric water continuum. J Chem Phys 2007;126:234301. <http://doi.org/10.1063/1.2746038>
589
590 [31]
591 Ptashnik I, Smith K, Shine K, Newnham D. Laboratory measurements of water vapor continuum
592 absorption in spectral region 5000 –5600 cm⁻¹: evidence for water dimers. Q J R Meteorol Soc
593 2004;130:2391–408. doi: 10.1256/qj.03.178
594
595 [32]
596 Paynter D, Ptashnik I, Shine K, Smith K. Pure water vapor continuum measurements between 3100
597 and 4400 cm⁻¹: evidence for water dimer absorption in near atmospheric conditions. Geophys Res
598 Lett 2007;34:L12808. doi: 10.1029/2007GL029259
599
600 [33]
601 Ptashnik IV. Evidence for the contribution of water dimers to the near-IR water vapor self-continuum.
602 J Quant Spectrosc Radiat Transf 2008;109:831–52. doi: 10.1016/j.jqsrt.2007.09.004

603
604 [34]
605 Ptashnik I, Shine KP, Viganin AA. Water vapor self-continuum and water dimers: 1. Analysis of recent
606 work. J Quant Spectrosc Radiat Transf 2011;112:1286–303. doi: 10.1016/j.jqsrt.2011.01.012
607
608 [35]
609 Birk M, Wagner G, Loos J, Shine KP. 3 μ m Water vapor self- and foreign- continuum: new method for
610 determination and new insights into the self- continuum. J Quant Spectrosc Radiat Transf
611 2020;253:107134. doi: 10.1016/j.jqsrt.2020.107134
612
613 [36]
614 Schofield DP, Kjaergaard HG. Calculated OH-stretching and HOH-bending vi- brational transitions in
615 the water dimer. Phys Chem Chem Phys 2003;5:310 0–5. doi: 10.1039/b304952c
616
617 [37]
618 Salmi T, Hänninen V, Garden AL, Kjaergaard HG, Tennyson J, Halonen L. Calculation of the O - H
619 stretching vibrational overtone spectrum of the water dimer. J Phys Chem A 2008;112:6305–12. doi:
620 10.1021/jp800754y. Correction to “Calculation of the O_H Stretching Vibrational Overtone Spectrum
621 of the Water Dimer”. J Phys Chem A 2008; 112:6305–6312. DOI: 10.1021/jp800754y |J Phys Chem A
622 2012;116:796–797. dx.doi.org/10.1021/jp210675h
623
624 [38]
625 Simonova AA, Ptashnik IV, Elsej J, McPheat RA, Shine KP, Smith KM. Water vapor self-continuum in
626 near-visible IR absorption bands: Measurements and semiempirical model of water dimer
627 absorption. J Quant Spectrosc Radiat Transf 2022;277:107957.
628 <https://doi.org/10.1016/j.jqsrt.2021.107957>.
629
630 [39]
631 Leshchishina O, Kassi S, Gordon IE, Rothman RL, Wang L, Campargue A. High sensitivity CRDS of the
632 $\alpha^1\Delta_g - X^3\Sigma_g^-(0 - 0)$ band of oxygen near 1.27 μ m: extended observations, quadrupole transitions,
633 hot bands and minor isotopologues. J Quant Spectrosc Radiat Transf 2010;111:2236-2245.
634 doi:10.1016/j.jqsrt.2010.05.014.
635
636 [40]
637 Mondelain D, Kassi S, Campargue A. Accurate laboratory measurement of the O₂ collision-induced
638 absorption band Near 1.27 μ m. J Geophys Res Atmos 2019;124:414–23. [10.1029/2018JD029317](https://doi.org/10.1029/2018JD029317).
639
640 [41]
641 Mendonca J, Strong K, Wunch D, Toon GC, Long DA, Hodges JT, et al. Using a speed-dependent Voigt
642 line shape to retrieve O₂ from total carbon column ob- serving network solar spectra to improve
643 measurements of XCO₂. Atmos Meas Tech 2019;12:35–50
644
645 [42]
646 Kassi S, Campargue A. Cavity Ring Down Spectroscopy with 5×10^{-13} cm⁻¹ sensitivity. J Chem Phys
647 2012;137:234201. <https://doi.org/10.1063/1.4769974>.
648
649 [43]
650 Konefał M, Mondelain D, Kassi S, Campargue A. High sensitivity spectroscopy of the O₂ band at 1.27
651 μ m: (I) pure O₂ line parameters above 7920 cm⁻¹. J Quant Spectrosc Radiat Transf 2020;241:106653.
652 <https://doi.org/10.1016/j.jqsrt.2019.106653>.
653

- 654 [44]
655 Gordon IE, Rothman LS, Hargreaves RJ, Hashemi R, Karlovets EV, Skinner FM, et al. The HITRAN2020
656 molecular spectroscopic database. *J Quant Spectrosc Radiat Transf* 2022;277:107949.
657 <https://doi.org/10.1016/j.jqsrt.2021.107949>
658
- 659 [45]
660 Koroleva AO, Odintsova TA, Tretyakov MY, Pirali O, Campargue A
661 The foreign-continuum absorption of water vapor in the far-infrared (50–500 cm^{-1}). *J Quant*
662 *Spectrosc Radiat Transf* 2021;261:107486. doi.org/10.1016/j.jqsrt.2020.107486
663
- 664 [46]
665 Ptashnik IV, Klimeshina TE, Solodov AA, Vigasin AA. Spectral composition of the water vapor self-
666 continuum absorption within 2.7 and 6.25 μm bands. *J Quant Spectrosc Radiat Transf* 2019;228:97–
667 105. doi: 10.1016/j.jqsrt.2019.02.024
668
- 669 [47]
670 Rocher-Casterline BE, Ch'ng LC, Mollner AK, Reisler H. Determination of the bond dissociation energy
671 (D_0) of the water dimer, $(\text{H}_2\text{O})_2$, by velocity map imaging. *J Chem Phys* 2011;134:211101.
672 <https://doi.org/10.1063/1.3598339>
673